SPEKTRA: Jurnal Fisika dan Aplikasinya
Volume 10, Issue 3, December 2025
Homepage: doi.org/10.21009/SPEKTRA

DOI: doi.org/10.21009/SPEKTRA.103.03

Comparative Study of Activation Functions and Image Resolution on ResNet-34 for Spiral Galaxy Spin Classification

Hafiz Indra Arwinata[1,*], Sultan Hadi Kusuma[1], Anton Timur Jaelani[2,3,4]

[1]*Astronomy Master Program, FMIPA, Institut Teknologi Bandung, Jl. Ganesa 10, Bandung 40132, Indonesia*
[2]*Astronomy Research Group and Bosscha Observatory, FMIPA, Institut Teknologi Bandung, Jl. Ganesa 10, Bandung 40132, Indonesia*
[3]*U-CoE AI-VLB, Institut Teknologi Bandung, Jl. Ganesa 10, Bandung 40132, Indonesia*
[4]*University Center of Excellence for Space Science, Technology and Innovation, Institut Teknologi Bandung, Jl. Ganesa 10, Bandung 40132, Indonesia*

*Corresponding Author Email: handranata13@gmail.com

Received: 18 August 2025
Revised: 14 November 2025
Accepted: 15 December 2025
Online: 22 December 2025
Published: 30 December 2025

SPEKTRA: Jurnal Fisika dan Aplikasinya
p-ISSN: 2541-3384
e-ISSN: 2541-3392

ABSTRACT

This study investigates the application of the Residual Network (ResNet-34) architecture for classifying spiral galaxy spin directions, specifically focusing on the comparative performance of activation functions and cross-dataset generalizability using data derived from the Dark Energy Spectroscopic Instrument Legacy Survey (DESI LS) and the Hyper Suprime Cam Subaru Strategic Program (HSC-SSP) surveys. The methodology ensures robustness by training each model configuration across 10 independent runs. The results demonstrate the clear superiority of the Rectified Linear Unit (ReLU) over the Hyperbolic Tangent (Tanh); ReLU-based models achieved a mean peak accuracy of 94.7% and required only less than 60 epochs to converge, significantly faster than Tanh's 120 epochs. Crucially, we found that models trained on lower-resolution DESI LS images exhibited superior robustness and generalizability compared to high-resolution-trained models, suggesting that low-resolution training acts as effective implicit regularization. This research provides critical design recommendations for efficient machine learning pipelines, particularly for upcoming facilities like the 3.8-meter telescope at Timau National Observatory (TNO), ensuring model stability and transferability across diverse survey conditions.

Keywords: spiral galaxies, spin direction, ResNet, ReLU, image resolution, deep learning

INTRODUCTION

The conventional explanation for the formation of spiral arm patterns in galaxies is the density wave theory [1]. However, recent simulations suggest that these patterns may instead result from amplified of swing processes driven by the shear motion within galaxies [2-3]. Determining the winding direction of spiral arms is essential, as it provides insight into galaxy formation by revealing the galaxies' spin vectors. According to tidal torque theory [4-6], galaxies acquire angular momentum in the early linear stages of structure formation from the tidal fields of neighbouring structures. This theory predicts a random distribution of galaxy spins direction; however, observed anomalies, such as anisotropies in winding directions, may indicate large-scale vorticity processes, including tidal interactions in galaxy clusters [7].

The angular momentum (spin) of galaxies, generated by tidal torque through misalignment between the protohalo inertia tensor and local gravitational tidal shear [4, 8-9], is a critical cosmological probe. It provides insight into neutrino mass, primordial chirality, and initial conditions of the Universe [10-14]. Motloch et al. [10] identified correlations between galaxy spins and the Universe's initial density field, though their research was constrained by a lack of spin measurements. Photometric studies infer the three-dimensional spin directions of spiral galaxies, often represented as circular disks. Observations confirm that spiral galaxies are trailing, with Z-wise spirals rotating clockwise [13]. Acurate measurement techniques are therefore required to enhance galaxy spin measurement.

Classifying spiral galaxies based on their spin direction can significantly advance our understanding of the Universe. One project dedicated to this goal is the Galaxy Zoo. Galaxy Zoo 1 (GZ1 – http://zoo1.galaxyzoo.org/) is a citizen science project that classified about 9×10^5 galaxies [14-15] from the Sloan Digital Sky Survey (SDSS) data [16-17], providing information on their spiral patterns (Z-wise or S-wise). However, the growing volume of data from extensive surveys, such as the Dark Energy Spectroscopic Instrument Legacy Imaging Surveys (DESI LS) [18] and the Hyper Suprime-Cam Subaru Strategic Program (HSC-SSP) [19], has made visual inspection increasingly impractical. Visual inspection is time-consuming, subjective, and lacks standardized criteria due to differing human interpretations of galaxy morphology. Consequently, machine learning-based classification methods have become necessary, with artificial neural networks (ANNs) emerging as a leading technique for image classification tasks in astrophysics [20-21].

This urgency is further amplified by upcoming and future photometric surveys, such as the Legacy Survey of Space and Time (LSST) by the Vera C. Rubin Observatory and the Euclid mission. These surveys are projected to deliver data volumes in the petabyte range, containing billions of galaxies [22-23]. Furthermore, this study is relevance to the future of Indonesian astronomy. The upcoming 3.8-meter telescope at Timau National Observatory (TNO) [24] need an efficient and reliable automated classification technique to maximize the scientific output and support cosmological research.

Although machine learning is a more efficient approach to galaxy morphology classification, it involves complex parameter tuning. The performance of convolutional neural networks (CNNs) is sensitive to critical architectural choices, notably the activation function and input

image resolution. Szandała [25] shows that the choice of activation functions has a significant impact on the model's training dynamics, convergence speed, and final accuracy. However, previous works on galaxy spin classification (e.g., [26] and [27]) have only employed a standard setup without a rigorous comparative assessment of the models, particularly concerning cross-dataset generalizability. Therefore, the primary goal of this research is to address this gap by investigating the performance of the residual network (ResNet) architecture when employing two common activation functions, namely the hyperbolic tangent function (Tanh) and the rectified linear unit (ReLU), and assessing the model's performance in cross-dataset generalization.

This paper discusses the dataset, model architecture, and results. The next section of the paper is the methodology, which describes the dataset, model architecture, and training process. The results, including the training and classification outcomes using the test data, are presented in the following section, followed by a discussion. The last section is the conclusion of this research.

METHODS

This section outlines the methodological steps taken in this research, from data acquisition to model training and testing. The overall research workflow is illustrated in FIGURE 1. The process begins with the selection of a data subset from the reduced GZ1 catalog by Jia et al. [27], followed by filtering based on specific criteria. The data of relevant images is then retrieved from the DESI LS and HSC-SSP surveys and re-verified through visual inspection to ensure the accuracy of the class labels. These verified images are subsequently fed into the ResNet-34 architecture. During the model training phase, data augmentation techniques are employed to increase data variability and improve generalization. The trained models are then tested using the test data. The training and testing results are systematically compared for the two activation functions, and a comprehensive cross-dataset generalization analysis is performed. The details of each step are explained in the following subsections.

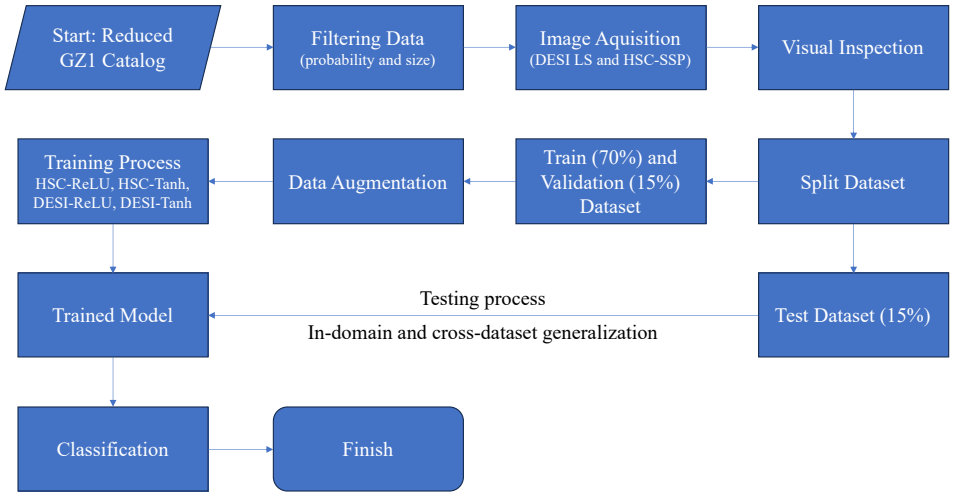

FIGURE 1. Methodology Flow Diagram. The overall workflow for this research, highlighting the systematic comparison between the ReLU and Tanh activation functions and the subsequent cross-dataset generalization analysis across the DESI LS and HSC-SSP surveys.

Data Source and Selection

In this paper, we used the reduced GZ1 dataset from Jia et al. [27] for training, validation, and testing. There dataset comprises a total of 173,097 galaxies, classified into three categories: *S-spirals*, *Z-spirals*, and *others*. The following sub-subsections give detail information about the DESI LS and the HSC-SSP surveys, and the selection criteria applied.

DESI LS

The Dark Energy Spectroscopic Instrument (DESI – https://data.desi.lbl.gov/doc/) is an instrument constructed for spectroscopic redshift surveys. The instrument is installed in the Mayall 4-meter telescope at the Kitt Peak National Observatory. Meanwhile, the DESI LS is a project that combines three individual and complementary projects: the Dark Energy Camera Legacy Survey, the Beijing–Arizona Sky Survey, and the Mayall z-band Legacy Survey [18]. This project aims to conduct an extragalactic survey from the northern hemisphere. This will also provide around 14,000 square degrees of sky coverage. There are three optical bands used in this project: *g, r,* and *z* filters. Currently, DESI LS has released public data ten times. In this paper, we used Data Release 9 [28].

HSC-SSP

The Subaru telescope is an 8.2-meter telescope located on the summit of Mauna Kea in Hawaii. One of the instruments installed in the telescope is the Hyper Suprime-Cam (HSC). This camera has a wide field of view (1.5°) that makes this instrument suitable for a survey program. The HSC-SSP Survey has three layers: the Wide layer that covers 1400 deg^2 of the sky, the Deep layer with sky coverage of 26 deg^2, and the UltraDeep layer with a total coverage of 3.5 deg^2 [19]. The wide layer has five broad bands: *g, r, i, z,* and *y* filters. For this paper, we used the wide layer of Public Data Release 3 that covers 600 deg^2 of the sky [29].

Selection Criteria

For our work, we selected only galaxies with a classification probability greater than 0.6 for each category, and possessing a Petrosian radius at 90% flux between 5 and 10 arcsec.

These galaxy images were then retrieved in JPEG format from the DESI LS and the HSC-SSP databases using the `EveryStamp` (https://tikk3r.github.io/EveryStamp/) and `Unagi` (https://github.com/dr-guangtou/unagi) cutout tools, respectively. To create color images, we employed the *grz* filters for the DESI LS data and *gri* filters for the HSC-SSP data. This filter selection was strictly based on two factors: data availability in each survey and maximize the volume of usable data. The DESI LS survey only provides data in the *g*, *r*, and *z* bands, while the HSC-SSP survey offered the highest volume of available images in the *g*, *r*, and *i* bands.

The selection criterion for the Petrosian radius, ranging from 5 to 10 arcsec, ensures that 90% of the galaxy light is contained within this aperture. Consequently, to prevent cropping of the largest selected galaxies, the image diameter must be at least 20 arcsec. The image size should also be carefully constrained to avoid rendering small galaxies too diminutively. The HSC-

SSP survey has a pixel scale of 0.168 arcsec/pixel, and DESI LS images retrieved using `EveryStamp` can be rescaled to match this. An input size of 160 × 160 pixels was selected as optimal, balancing the preservation of morphological features with computational efficiency, consistent with Jia et al. [27]. Examples of these images are presented in FIGURE 2.

We also performed visual inspections to ensure the accuracy of the classification process. After applying all selection criteria and visual inspections, we obtained a final sample consisting of 2,123 *S-spiral* galaxies, 2,072 *Z-spiral* galaxies, and 2,205 galaxies classified as *others*. Crucially, the number of *S-spiral* and *Z-spiral* galaxies is nearly balanced, which means that explicit handling of data imbalance was not necessary for the spin classification task. The final dataset was then split into 70% for training, 15% for validation, and 15% for testing subsets.

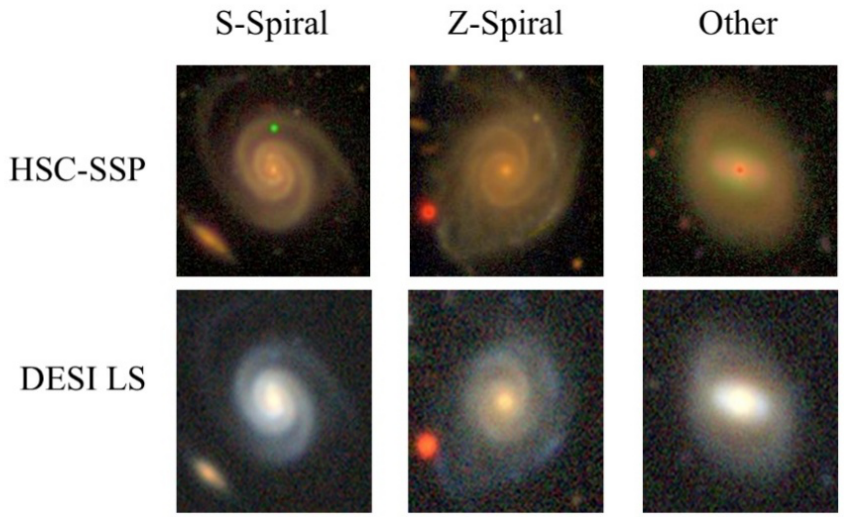

FIGURE 2. The samples image of S-spiral, Z-spiral, and other galaxies from HSC-SSP (top panel) and DESI LS (bottom panel). The images from HSC-SSP have a higher resolution compared to those from DESI LS.

Network Architecture

This research focuses on classifying galaxies into *Z-spiral*, *S-spiral*, and *others* using a ResNet. ResNet addresses the degradation issue observed in very deep networks, as reported by He & Sun [30], significantly enhancing performance in computer vision tasks [31]. It resolves this problem by introducing residual connections, enabling network layers to approximate the identity function. This approach prevents network performance from saturating or deteriorating with increasing depth. As a result, deeper networks can match or surpass the accuracy of shallower ones, making ResNet particularly reliable and highly effective, an essential feature for astrophysical image classification.

As the primary objective of this research is to evaluate the impact of different non-linearities on model performance and generalization, this study explicitly compares two widely-adopted activation functions applied within the convolutional layers:

1. ReLU: This function is defined as $f(x) = \max(0, x)$. The ReLU is a function that returns the input value x if x is positive, and it returns zero if x is zero or negative.
2. Tanh: This function is defined mathematically as $f(x) = \frac{e^{x} - e^{-x}}{e^{x} + e^{-x}}$ The output values of Tanh are within the [-1, 1] range, which is zero-centered. However, it is susceptible to the saturation problem, where gradients approach zero for very large or very small inputs.

We utilized the network structure outlined in TABLE 1 to develop our model using `PyTorch` [32], based on the ResNet-34 architecture [31]. We included dropout layers before the fully connected layers. Additionally, we applied the softmax function to compute the probabilities for the three classification categories.

TABLE 1. The architecture of our ResNet-34.

Layer Name	Output Size	34-layer ResNet
conv1	80 × 80 × 64	7 × 7, 64, stride 2
conv2_x	40 × 40 × 64	3 × 3 max pool, stride 2 $\begin{bmatrix} 1 \times 1, 64 \\ 3 \times 3, 64 \end{bmatrix} \times 3$
conv3_x	20 × 20 × 128	$\begin{bmatrix} 1 \times 1, 128 \\ 3 \times 3, 128 \end{bmatrix} \times 4$
conv4_x	10 × 10 × 256	$\begin{bmatrix} 1 \times 1, 256 \\ 3 \times 3, 256 \end{bmatrix} \times 6$
conv5_x	5 × 5 × 512	$\begin{bmatrix} 1 \times 1, 512 \\ 3 \times 3, 512 \end{bmatrix} \times 3$
fc	3	Average pool, output 1 × 1 × 512, dropout, 512-512-64-64-3 fully connected

Training Process

The inputs to our model are three-channel RGB images of shape $30 \times 160 \times 160$. To ensure generalization, we applied data augmentation techniques during training. These techniques included:

1. Random rotation of galaxies by angles drawn from a uniform distribution U (−90°, +90°).
2. Random adjustments to brightness, contrast, saturation, and hue, sampled from uniform distributions.
    a. Brightness: U (0.5, 1.5)
    b. Contrast: U (0.5, 1.5)
    c. Saturation: U (0.8, 1.8)

d. Hue: U (−0.1, 0.1).

All models were trained using the Adam Optimizer on the cross-entropy loss function. The training process utilized an initial learning rate of 1×10^{-5} with a batch size of 32. The models using the ReLU activation function were trained for 60 epochs, while those using the Tanh activation function required a longer training duration of 120 epochs to achieve convergence. Training was executed on the Kaggle (https://www.kaggle.com/) platform, utilizing a single NVIDIA Tesla P100 GPU. The typical training time for the ReLU-based models (60 epochs) was approximately 30 minutes, while the Tanh-based models (120 epochs) required approximately one hour.

To account for variance in the training process and ensure the robustness of the results, each model configuration was independently trained and evaluated 10 times. The performance metrics reported in results section are the mean values derived from these 10 training runs, alongside the calculated standard deviation to quantify the uncertainty.

RESULTS AND DISCUSSIONS

The training and validation results in the left panels of FIGURE 3 show that the ReLU models achieved relatively high accuracy; however, signs of overfitting appeared around the 25th epoch. In order to prevent overfitting, we selected the model from the 25th epoch for testing. In contrast, the right panels of FIGURE 2 show that models using Tanh activation function achieved lower accuracy and exhibit higher loss values. Overfitting was observed near the 100th epoch, so we used the model from that epoch for testing. A summary of the training and validation of accuracy and loss for all models is presented in TABLE 2. Our results indicate that models using ReLU consistently outperformed those using Tanh, and models trained on HSC-SSP images achieved higher overall accuracy. The low standard deviation observed across all models confirms that the reported results are statistically stable.

The mean peak accuracy of our model on the HSC-SSP dataset is 94.7%, which is slightly lower than the 97.5% reported by Tadaki et al. [26] on the same survey data. This difference can be attributed to several key methodological distinctions. Their research employed a shallower CNN trained on monochromatic 64×64 HSC images that were pre-selected to contain unambiguously clear *Z-spirals*, *S-spirals*, and *non-spirals*. This rigid data selection most likely improved their accuracy. In addition, their data augmentation process is quite different from ours, especially in the variation of the gamma parameter and the addition of flipped data, which can also affect the accuracy. Conversely, our ResNet-34 model shows competitive performance when compared to the more complex Chirality Equivariant Residual Network (CE-ResNet) used by Jia et al. [27]. Our loss result for the DESI LS data is notably lower than the finding reported by Jia et al. [27], confirming the efficiency of our model configuration.

TABLE 2. The training and validation accuracy and loss for all models, based on the 25th epoch for ReLU and 100th epoch for tanh.

Data	Model Name	Train		Validation	
		Accuracy	Loss	Accuracy	Loss
HSC-SSP	HSC-ReLU	0.947 ± 0.004	0.137 ± 0.008	0.947 ± 0.007	0.144 ± 0.016
	HSC-Tanh	0.895 ± 0.005	0.269 ± 0.008	0.908 ± 0.008	0.232 ± 0.017
DESI LS	DESI-ReLU	0.926 ± 0.003	0.189 ± 0.005	0.914 ± 0.007	0.216 ± 0.014
	DESI-Tanh	0.864 ± 0.004	0.346 ± 0.008	0.874 ± 0.009	0.323 ± 0.017

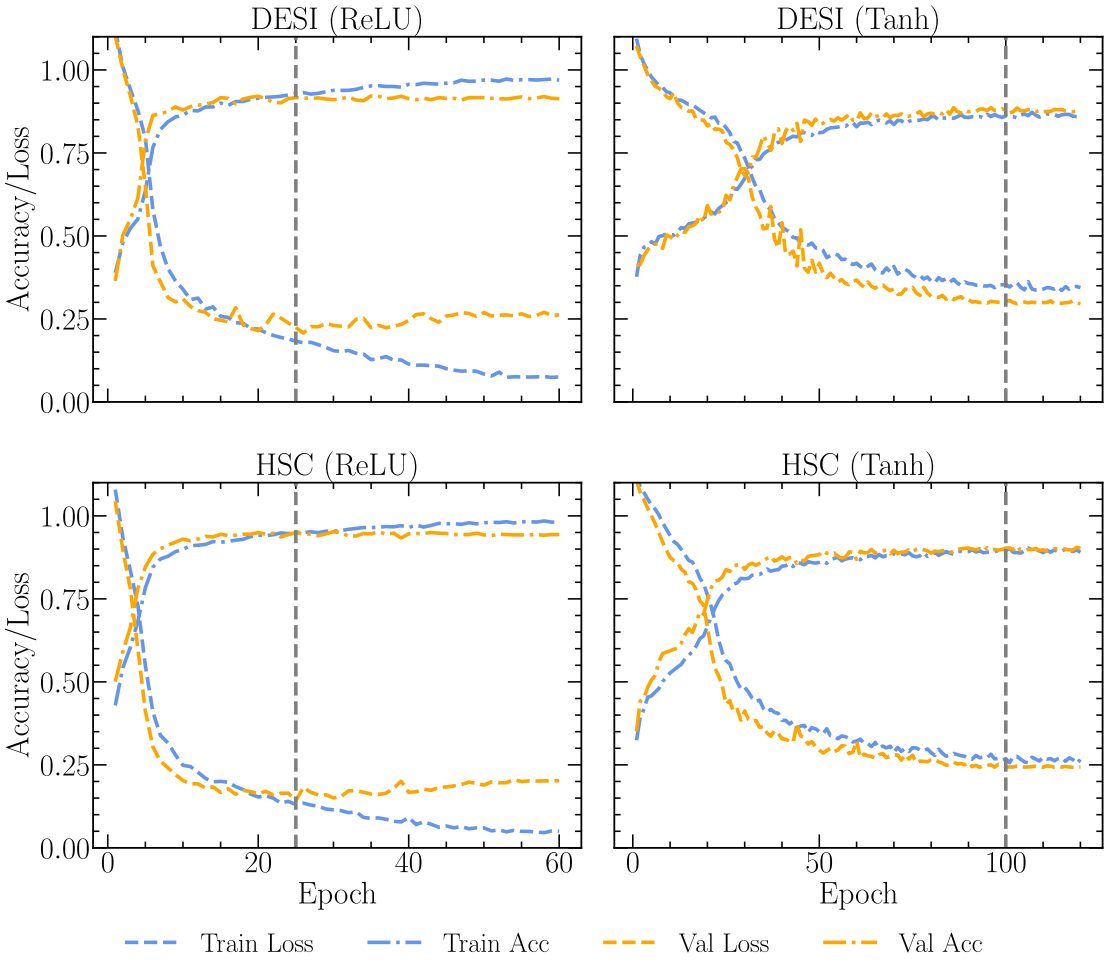

FIGURE 3. The training (train) loss and validation (val) loss of our models, evaluated on DESI LS images (top panels) and HSC-SSP images (bottom panels). Training was terminated after 60 epochs for models using the ReLU activation function (left panels) and after 120 epochs for those using the tanh activation function (right panels). The vertical grey lines indicate the epochs at which the models were evaluated on the test data.

To further evaluate model performance and robustness, we conducted a comprehensive testing phase. Testing was first performed using HSC-SSP images to HSC-trained models and DESI LS images on DESI-trained models, allowing us to in-domain performance. Additionally, we performed cross-dataset evaluations: HSC-trained models were tested on DESI LS images and vice versa. This approach enabled us to assess the consistency and generalizability of our models accros different datasets. A summary of the testing results is presented in TABLE 3.

TABLE 3. The accuracy and loss from the testing process for all models.

Data Source	Model Name	Accuracy	Loss
HSC-SSP	HSC-ReLU	0.951 ± 0.003	0.134 ± 0.007
	HSC-Tanh	0.912 ± 0.005	0.235 ± 0.007
	DESI-ReLU	0.916 ± 0.010	0.223 ± 0.031
	DESI-Tanh	0.790 ± 0.050	0.529 ± 0.086
DESI LS	HSC-ReLU	0.571 ± 0.054	1.320 ± 0.165
	HSC-Tanh	0.386 ± 0.015	1.709 ± 0.174
	DESI-ReLU	0.919 ± 0.006	0.207 ± 0.013
	DESI-Tanh	0.893 ± 0.005	0.288 ± 0.006

The test results confirm that models using the ReLU activation function yielded higher and more consistent accuracy compared to those using the Tanh. The superior performance of the ReLU over the Tanh in our models is strongly supported by deep learning literature. As noted by Szandała [25], the primary advantage of ReLU is its ability to mitigate the vanishing gradient problem, which is prevalent in 'S'-shaped functions like Tanh. ReLU maintains a constant non-zero gradient for positive inputs, ensuring that the error signal propagates efficiently during backpropagation, leading to faster and more stable convergence [25]. This efficiency is empirically proven in our results: the ReLU models required less than 60 epochs to converge, while the Tanh function required a significantly longer duration of 120 epochs to achieve comparable stability. Thus, for complex, multi-layer convolutional tasks like galaxy classification, the non-saturating nature of ReLU makes it a substantially more effective choice.

A crucial finding of this research, extending beyond activation functions, concerns the impact of image resolution on cross-dataset generalizability. Notably, HSC-trained models experienced a significant performance drop when tested with DESI LS data images, whereas DESI-trained models maintained relatively high accuracy when tested on HSC-SSP images. These results show that models trained with lower-resolution images exhibit higher robustness and generalization compared to models trained with higher-resolution images. This effect is interpreted as implicit regularization, where lower resolution inherently forces the model to focus on large-scale, invariable morphological features and ignore minor details. Conversely, models trained with high resolution overfit the small details of HSC-SSP images. When these specific high-frequency features are absent or changed in the DESI LS test set, the classification confidence of the model will collapse, indicating poor generalization.

As shown in TABLE 2 and TABLE 3, our models exhibited relatively high loss values. To investigate this, we analyzed the confusion matrix from the testing phase (see FIGURE 3a). The matrix reveals that most mislabeling involved galaxies from the *others* category, which were often incorrectly labeled as either *S-spiral* or *Z-spiral* galaxies. These mislabellings may be attributed to the small size of the galaxies' images or the lack of distinct spiral arm features, which makes the classification task more challenging. Furthermore, possible biases in the initial visual classification process could contribute to inaccuracies in the training labels.

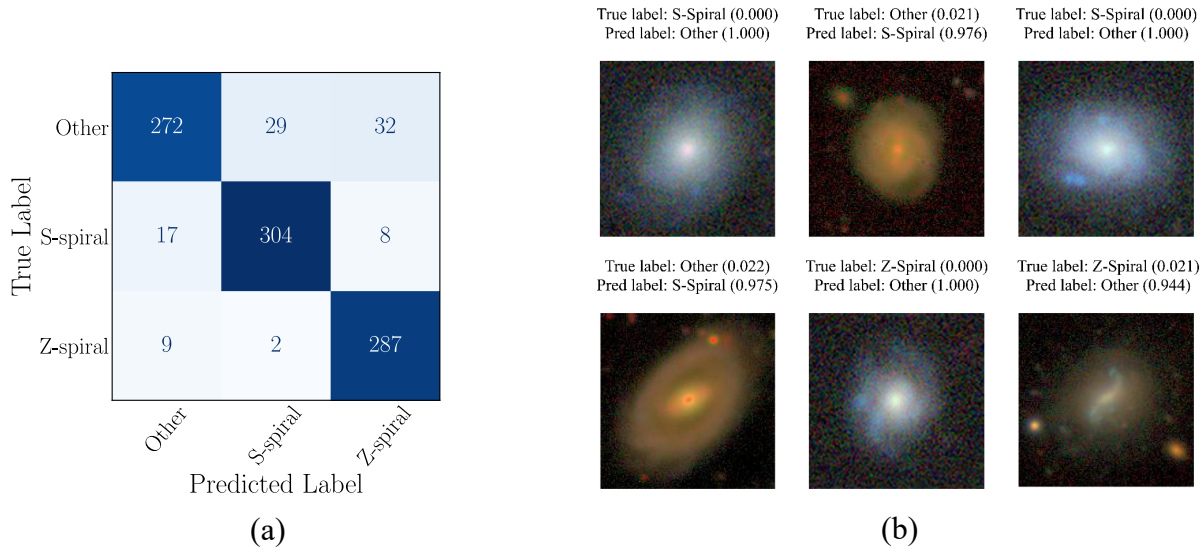

FIGURE 3. (a) Sample of confusion matrix from testing phase. (b) Sample mislabeling galaxies from DESI LS and HSC-SSP images.

CONCLUSION

This study concludes that both the activation function and image resolution play a critical role in classifying galaxy spin directions. Specifically, the ResNet-34 architecture paired with the ReLU activation function consistently delivered high classification accuracy of up to 94.7%, along with faster and more stable convergence, outperforming the Tanh activation function. Additionally, a key insight for future surveys is that models trained on lower-resolution DESI LS images showed significantly better generalization when tested on high-resolution HSC-SSP data, highlighting the value of low-resolution training for cross-dataset robustness. These findings offer practical recommendations for next-generation Indonesian astronomical facilities, such as the 3.8-meter telescope at TNO.

Future research can be improved in several key areas: increasing the size and diversity of the training dataset to enhance model robustness, exploring the effectiveness of more advanced and contemporary neural network architectures, and implementing bias-reduction strategies such as image inversion for Z-spiral and S-spiral galaxies. These improvements aim to support fairer and more reliable classification across various morphological types.

ACKNOWLEDGEMENTS

We acknowledge the support of the Program Penelitian, Pengabdian Masyarakat, dan Inovasi (PPMI) ITB 2025 for this research.

The Hyper Suprime-Cam (HSC) collaboration includes the astronomical communities of Japan and Taiwan, and Princeton University. The HSC instrumentation and software were developed by the National Astronomical Observatory of Japan (NAOJ), the Kavli Institute for the Physics and Mathematics of the Universe (Kavli IPMU), the University of Tokyo, the High Energy Accelerator Research Organization (KEK), the Academia Sinica Institute for Astronomy and Astrophysics in Taiwan (ASIAA), and Princeton University. Funding was

contributed by the FIRST program from the Japanese Cabinet Office, the Ministry of Education, Culture, Sports, Science and Technology (MEXT), the Japan Society for the Promotion of Science (JSPS), Japan Science and Technology Agency (JST), the Toray Science Foundation, NAOJ, Kavli IPMU, KEK, ASIAA, and Princeton University.

This paper makes use of software developed for Vera C. Rubin Observatory. We thank the Rubin Observatory for making their code available as free software at http://pipelines.lsst.io/.

This paper is based on data collected at the Subaru Telescope and retrieved from the HSC data archive system, which is operated by the Subaru Telescope and Astronomy Data Center (ADC) at NAOJ. Data analysis was in part carried out with the cooperation of Center for Computational Astrophysics (CfCA), NAOJ. We are honored and grateful for the opportunity of observing the Universe from Maunakea, which has the cultural, historical and natural significance in Hawaii.

The Legacy Surveys consist of three individual and complementary projects: the Dark Energy Camera Legacy Survey (DECaLS; Proposal ID #2014B-0404; PIs: David Schlegel and Arjun Dey), the Beijing-Arizona Sky Survey (BASS; NOAO Prop. ID #2015A-0801; PIs: Zhou Xu and Xiaohui Fan), and the Mayall z-band Legacy Survey (MzLS; Prop. ID #2016A-0453; PI: Arjun Dey). DECaLS, BASS and MzLS together include data obtained, respectively, at the Blanco telescope, Cerro Tololo Inter-American Observatory, NSF's NOIRLab; the Bok telescope, Steward Observatory, University of Arizona; and the Mayall telescope, Kitt Peak National Observatory, NOIRLab. Pipeline processing and analyses of the data were supported by NOIRLab and the Lawrence Berkeley National Laboratory (LBNL). The Legacy Surveys project is honored to be permitted to conduct astronomical research on Iolkam Du'ag (Kitt Peak), a mountain with particular significance to the Tohono O'odham Nation.

NOIRLab is operated by the Association of Universities for Research in Astronomy (AURA) under a cooperative agreement with the National Science Foundation. LBNL is managed by the Regents of the University of California under contract to the U.S. Department of Energy.

This project used data obtained with the Dark Energy Camera (DECam), which was constructed by the Dark Energy Survey (DES) collaboration. Funding for the DES Projects has been provided by the U.S. Department of Energy, the U.S. National Science Foundation, the Ministry of Science and Education of Spain, the Science and Technology Facilities Council of the United Kingdom, the Higher Education Funding Council for England, the National Center for Supercomputing Applications at the University of Illinois at Urbana-Champaign, the Kavli Institute of Cosmological Physics at the University of Chicago, Center for Cosmology and Astro-Particle Physics at the Ohio State University, the Mitchell Institute for Fundamental Physics and Astronomy at Texas A&M University, Financiadora de Estudos e Projetos, Fundacao Carlos Chagas Filho de Amparo, Financiadora de Estudos e Projetos, Fundacao Carlos Chagas Filho de Amparo a Pesquisa do Estado do Rio de Janeiro, Conselho Nacional de Desenvolvimento Cientifico e Tecnologico and the Ministerio da Ciencia, Tecnologia e Inovacao, the Deutsche Forschungsgemeinschaft and the Collaborating Institutions in the Dark Energy Survey. The Collaborating Institutions are Argonne National Laboratory, the University of California at Santa Cruz, the University of Cambridge, Centro

de Investigaciones Energeticas, Medioambientales y Tecnologicas-Madrid, the University of Chicago, University College London, the DES-Brazil Consortium, the University of Edinburgh, the Eidgenossische Technische Hochschule (ETH) Zurich, Fermi National Accelerator Laboratory, the University of Illinois at Urbana-Champaign, the Institut de Ciencies de l'Espai (IEEC/CSIC), the Institut de Fisica d'Altes Energies, Lawrence Berkeley National Laboratory, the Ludwig Maximilians Universitat Munchen and the associated Excellence Cluster Universe, the University of Michigan, NSF's NOIRLab, the University of Nottingham, the Ohio State University, the University of Pennsylvania, the University of Portsmouth, SLAC National Accelerator Laboratory, Stanford University, the University of Sussex, and Texas A&M University.

BASS is a key project of the Telescope Access Program (TAP), which has been funded by the National Astronomical Observatories of China, the Chinese Academy of Sciences (the Strategic Priority Research Program "The Emergence of Cosmological Structures" Grant # XDB09000000), and the Special Fund for Astronomy from the Ministry of Finance. The BASS is also supported by the External Cooperation Program of Chinese Academy of Sciences (Grant # 114A11KYSB20160057), and Chinese National Natural Science Foundation (Grant # 12120101003, # 11433005).

The Legacy Survey team makes use of data products from the Near-Earth Object Wide-field Infrared Survey Explorer (NEOWISE), which is a project of the Jet Propulsion Laboratory/California Institute of Technology. NEOWISE is funded by the National Aeronautics and Space Administration.

The Legacy Surveys imaging of the DESI footprint is supported by the Director, Office of Science, Office of High Energy Physics of the U.S. Department of Energy under Contract No. DE-AC02-05CH1123, by the National Energy Research Scientific Computing Center, a DOE Office of Science User Facility under the same contract; and by the U.S. National Science Foundation, Division of Astronomical Sciences under Contract No. AST-0950945 to NOAO.

REFERENCES

[1] C. C. Lin and F. H. Shu, "On the spiral structure of disk galaxies," *Astrophys. J.*, vol. 140, p. 646, Aug. 1964, doi: 10.1086/147955.

[2] J. Baba, T. R. Saitoh, and K. Wada, "Dynamics of non-steady spiral arms in disk galaxies," *Astrophys. J.*, vol. 763, no. 1, p. 46, 2013, doi: 10.1088/0004-637X/763/1/46.

[3] C. Dobbs and J. Baba, "Dawes Review 4: Spiral structures in disc galaxies," *Publ. Astron. Soc. Aust.*, vol. 31, p. e035, 2014, doi: 10.1017/pasa.2014.31.

[4] A. G. Doroshkevich, "Spatial structure of perturbations and origin of galactic rotation in fluctuation theory," *Astrophysics*, vol. 6, 1970, doi: 10.1007/BF01001625.

[5] P. J. E. Peebles, "Origin of the angular momentum of galaxies," *Astrophys. J.*, vol. 155, p. 393, Feb. 1969, doi: 10.1086/149876.

[6] S. D. M. White, "Angular momentum growth in protogalaxies," *Astrophys. J.*, vol. 286, pp. 38–41, Nov. 1984, doi: 10.1086/162573.

[7] H. Sugai and M. Iye, "A statistical search for correlations of rotational spin angular momentum between galaxies," *Mon. Not. R. Astron. Soc.*, vol. 276, no. 1, pp. 327–335, Sep. 1995, doi: 10.1093/mnras/276.1.327.

[8] J. Lee and U.-L. Pen, "Cosmic shear from galaxy spins," *Astrophys. J.*, vol. 532, no. 1, p. L5, 2000, doi: 10.1086/312556.

[9] J. Lee and U.-L. Pen, "Galaxy spin statistics and spin-density correlation," *Astrophys. J.*, vol. 555, no. 1, p. 106, 2001, doi: 10.1086/321472.
[10] P. Motloch, H.-R. Yu, U.-L. Pen, and Y. Xie, "An observed correlation between galaxy spins and initial conditions," *Nat. Astron.*, vol. 5, no. 3, pp. 283–288, Jul. 2021, doi: 10.1038/s41550-020-01262-3.
[11] H.-R. Yu *et al*., "Probing primordial chirality with galaxy spins," *Phys. Rev. Lett.*, vol. 124, no. 10, p. 101302, Mar. 2020, doi: 10.1103/PhysRevLett.124.101302.
[12] H.-R. Yu, U.-L. Pen, and X. Wang, "Parity-odd neutrino torque detection," *Phys. Rev. D*, vol. 99, no. 12, p. 123532, Jun. 2019, doi: 10.1103/PhysRevD.99.123532.
[13] M. Iye, K. Tadaki, and H. Fukumoto, "Spin parity of spiral galaxies. I. Corroborative evidence for trailing spirals," *Astrophys. J.*, vol. 886, no. 2, p. 133, Nov. 2019, doi: 10.3847/1538-4357/ab4a18.
[14] C. J. Lintott *et al*., "Galaxy Zoo: Morphologies derived from visual inspection of galaxies from the Sloan Digital Sky Survey," *Mon. Not. R. Astron. Soc.*, vol. 389, no. 3, pp. 1179–1189, Jul. 2008, doi: 10.1111/j.1365-2966.2008.13689.x.
[15] C. Lintott *et al*., "Galaxy Zoo 1: Data release of morphological classifications for nearly 900 000 galaxies," *Mon. Not. R. Astron. Soc.*, vol. 410, no. 1, pp. 166–178, Jan. 2011, doi: 10.1111/j.1365-2966.2010.17432.x.
[16] K. N. Abazajian *et al*., "The seventh data release of the Sloan Digital Sky Survey," *Astrophys. J. Suppl. Ser.*, vol. 182, no. 2, p. 543, 2009, doi: 10.1088/0067-0049/182/2/543.
[17] R. Ahumada *et al*., "The sixteenth data release of the Sloan Digital Sky Surveys," *Astrophys. J. Suppl. Ser.*, vol. 249, no. 1, p. 3, 2020, doi: 10.3847/1538-4365/ab929e.
[18] A. Dey *et al*., "Overview of the DESI legacy imaging surveys," *Astron. J.*, vol. 157, no. 5, p. 168, 2019, doi: 10.3847/1538-3881/ab089d.
[19] H. Aihara *et al*., "The Hyper Suprime-Cam SSP survey: Overview and survey design," *Publ. Astron. Soc. Jpn.*, vol. 70, no. SP1, p. S4, Jan. 2018, doi: 10.1093/pasj/psx066.
[20] M. A. Hayat *et al*., "Self-supervised representation learning for astronomical images," *Astrophys. J. Lett.*, vol. 911, no. 2, p. L33, 2021, doi: 10.3847/2041-8213/abf2c7.
[21] S. He *et al*., "Learning to predict the cosmological structure formation," *Proc. Natl. Acad. Sci. U.S.A.*, vol. 116, no. 28, pp. 13825–13832, 2019, doi: 10.1073/pnas.1821458116.
[22] Ž. Ivezić *et al*., "LSST: From science drivers to reference design and anticipated data products," *Astrophys. J.*, vol. 873, no. 2, p. 111, 2019, doi: 10.3847/1538-4357/ab042c.
[23] Euclid Collaboration *et al*., "Euclid," *Astron. Astrophys.*, vol. 697, 2025, doi: 10.1051/0004-6361/202450810.
[24] E. S. Mumpuni *et al*., "Future astronomy facilities in Indonesia," *Nat. Astron.*, vol. 2, no. 12, pp. 930–932, 2018, doi: 10.1038/s41550-018-0642-6.
[25] T. Szandała, "Review and comparison of commonly used activation functions for deep neural networks," in *Bio-inspired Neurocomputing*, A. K. Bhoi *et al*., Eds. Singapore: Springer, 2021, pp. 203–224, doi: 10.1007/978-981-15-5495-7_11.
[26] K. Tadaki *et al*., "Spin parity of spiral galaxies II," *Mon. Not. R. Astron. Soc.*, vol. 496, no. 4, pp. 4276–4286, Aug. 2020, doi: 10.1093/mnras/staa1880.
[27] H. Jia, H.-M. Zhu, and U.-L. Pen, "Galaxy spin classification. I," *Astrophys. J.*, vol. 943, no. 1, p. 32, 2023, doi: 10.3847/1538-4357/aca8aa.
[28] D. Schlegel *et al*., "DESI legacy imaging surveys data release 9," in *Proc. AAS Meeting*, vol. 237, Jan. 2021, p. 235.03.
[29] H. Aihara *et al*., "Third data release of the Hyper Suprime-Cam Subaru Strategic Program," *Publ. Astron. Soc. Jpn.*, vol. 74, no. 2, pp. 247–272, Apr. 2022, doi: 10.1093/pasj/psab122.
[30] K. He and J. Sun, "Convolutional neural networks at constrained time cost," in *Proc. IEEE Conf. Comput. Vis. Pattern Recognit. (CVPR)*, 2015, pp. 5353–5360, doi: 10.1109/CVPR.2015.7299173.
[31] K. He, X. Zhang, S. Ren, and J. Sun, "Deep residual learning for image recognition," in *Proc. IEEE Conf. Comput. Vis. Pattern Recognit. (CVPR)*, 2016, pp. 770–778, doi: 10.1109/CVPR.2016.90.

[32] A. Paszke *et al*., "PyTorch: An imperative style, high-performance deep learning library," in *Adv. Neural Inf. Process. Syst.*, 2019.